Tight-binding Hamiltonians for Sr-filled ruthenates: Application to the gap anisotropy and Hall coefficient in Sr_2RuO_4

I. I. Mazin, D. A. Papaconstantopoulos, and D. J. Singh
Center for Computational Materials Science, Naval Research Laboratory, Washington, D.C. 20375
(Received 27 July 1999)

Accurate orthogonal tight-binding Hamiltonians are constructed for ferromagnetic $SrRuO_3$ and the layered perovskite superconductor, Sr_2RuO_4 by fitting to all-electron full-potential local density band structures obtained by the linearized augmented plane-wave method. These Hamiltonians allow the band structure to be computed on very fine meshes in the Brillouin zone at low cost, and additionally have an analytic form for band velocities, while retaining the accuracy of the full-potential electronic structure calculations. This greatly facilitates calculation of transport and superconducting parameters related to the fermiology. These features are exploited to calculate the Hall coefficient and vortex lattice geometry for Sr_2RuO_4 with fine integration meshes. We find the upper limit for the interband order parameter anisotropy to be compatible with the observed square geometry. We also find that the sign reversal of the Hall coefficient can be explained in a conventional way if the bands are shifted by a few mRy so as to match the experimental de Haas–van Alphen areas exactly, *and* the temperature dependence of the relaxation time is strongly dependent on the band character.

INTRODUCTION

The Sr-Ru-O system initially attracted interest because of technological applications as perovskite substrates. In the last few years, however, the unique electronic properties of ruthenates made them objects of interest from the point of view of fundamental solid-state physics. The root compound for this system is the pseudocubic perovskite $SrRuO_3$. This material has an orthorhombic Pbnm ($GdFeO_3$) structure, and is a strong ferromagnet. It is characterized by unusual transport properties (so-called ''bad metal'' behavior), unusually strong coupling between the spin and charge degrees of freedom, and substantial involvement of oxygen in its magnetic properties. Sr_2RuO_4 occurs in a body-centered tetragonal K_2NiF_4 structure and is superconducting at a temperature of 1.5 K. It is generally accepted now that the superconductivity of Sr_2RuO_4 is unconventional and most likely triplet. A number of researchers expressed an opinion that ruthenates, or at least some of them, may be strongly correlated systems close to Mott-Hubbard transition. On the other hand, unlike common strongly correlated materials ($3d$ oxides, high-T_c cuprates), the physical properties of ruthenates are well described by conventional density functional theory, and their unusual transport properties are likely to be due to strong magnetic interactions and magnetic scattering.

Density-functional electronic structure calculations have been reported for cubic and orthorhombic $SrRuO_3$ (Ref. 1) and for Sr_2RuO_4,[2,3] using the general potential linearized augmented plane-wave method (LAPW). An analysis of the resulting electronic structure was given in Refs. 4 and 5. At the moment, essentially all observable properties that could be reliably calculated from the electronic structure results agree well with the experiment. On the other hand, there are several properties of this material that cannot be reliably obtained directly with the LAPW method due to the high-computational cost. At the same time, there is substantial interest among both theorists (as a starting point for many body models) and experimentalists in having a simple, fast tight-binding model that would accurately describe the local-density approximation (LDA) electronic structure near the Fermi level.[6,7] Existing tight-binding models[5,8] do not reproduce accurately enough the details of the fermiology, e.g., the degree of nesting. For this reason we have performed highly accurate tight-binding parametrizations of this system by fitting to LAPW results.

CONSTRUCTION OF THE TIGHT-BINDING HAMILTONIANS

For the cubic $SrRuO_3$ we constructed orthogonal tight-binding (TB) Hamiltonians by fitting to the spin-polarized band structure of Ref. 1. We followed a procedure similar to the one used for other oxide perovskites[9], based on 14 LAPW bands for each of 165 **k** points in the irreducible Brillouin zone. Our TB Hamiltonian results in a 14×14 secular equation based on the *d*-Ru and *p*-O orbitals. This

TABLE I. Slater-Koster parameters for the cubic $SrRuO_3$ (mRy).

	Ru onsite		O onsite		Ru-Ru			O-O		Ru-O		O-O	
Spin	t_{2g}	e_g	p_σ	p_π	$dd\sigma$	$dd\pi$	$dd\delta$	$pp\sigma$	$pp\pi$	$pd\sigma$	$pd\pi$	$pp\sigma$ [a]	$pp\pi$ [a]
↑	493	738	307	405	−28	−12	1	43	−11	168	−94	14	−4
↓	534	772	316	420	−27	−11	1	43	−11	165	−97	14	−5

[a]Second nearest neighbors.

TABLE II. Slater-Koster parameters for Sr_2RuO_4 (mRy).

Ru onsite			O1 onsite	O2 onsite		Sr onsite			Ru-Ru			O1-O1		O2-O2		O1-O2		
xy	yz,zx	e_g	p	z	x,y	xy	yz,zx	e_g	$dd\sigma$	$dd\pi$	$dd\delta$	$pp\sigma$	$pp\pi$	$pp\sigma$	$pp\pi$	$pp\sigma$	$pp\pi$	$pp\sigma$ [a]
487	516	659	338	392	436	1032	1318	1874	−7	−3	−6	37	−7	7	4	44	−18	−7

Sr-Sr		Sr-Ru		O1-Sr		O1-Ru		O2-Sr		O2-Ru		
$dd\pi$	$dd\sigma$	$dd\pi$	$dd\delta$	$pd\sigma$	$pd\pi$	$pd\sigma$	$pd\pi$	$pd\sigma$	$pd\pi$	$pd\sigma$	$pd\pi$	$pd\sigma$ [a]
39	−80	−7	−38	−47	110	190	96	61	−58	160	68	17

[a]Second nearest neighbors.

Hamiltonian contains 11 first and 2 second nearest-neighbor Slater-Koster parameters (listed in Table I) for each spin determined by least-squares fitting to the LAPW results. The overall rms error for all 14 bands was 14 mRy. This high level of accuracy is demonstrated in our energy band and densities of states figures discussed in the next section. As can be seen from Table I, we have included the crystal field splitting $e_g - t_{2g}$ on the Ru d states, which is 3.34 eV (↑) and 3.23 eV (↓). There is also significant crystal-field splitting $p_\pi - p_\sigma$ on the oxygen site, 1.33 eV (↑) and 1.41 eV (↓) (a similar effect exists in manganite perovskites, cf. Ref. 10). The exchange splitting for Ru is relatively small: 0.57 eV (t_{2g}) and 0.45 eV (e_g). We also have exchange splitting on the O sites (0.12 eV for p_σ and 0.20 eV for p_π), in accord with the general role of Ru-O hybridization in ruthenates, as discussed in Ref. 4. The strongest interactions in the system are (Table I) the Ru-O $pd\sigma$ and $pd\pi$, as expected. We also note that in order to obtain a good fit we had to include the second nearest $pp\sigma$ and $pp\pi$ interactions. Another observation that can be made from Table I is that the rigid-band Stoner picture describes the physics of magnetic splitting rather well: there is hardly any difference between the hopping integral in the spin up and in the spin down channels.

For Sr_2RuO_4, we followed a similar procedure to construct the orthogonal Hamiltonian. The details are as follows. We fitted to the LAPW results of Ref. 2 using 18 bands for each of 207 **k** points in the irreducible Brillouin zone. The size of our Hamiltonian matrix became 27×27 based on the d-Sr, d-Ru and p-O orbitals. Having in mind applications to superconductivity theory, we aimed at having a virtually perfect fit in the window of ±1 eV around the Fermi level. For that inclusion of the d-Sr orbitals was unavoidable. This Hamiltonian contains 30 first and 2 second nearest-neighbor parameters. Since we used an orthogonal TB model, the physical nonorthogonality between d-Ru and p-O orbitals (which have bigger overlaps than other orbitals in the system) spills over into nonzero second nearest-neighbor parameters in an orthogonal Hamiltonian, specifically Ru-O2 $pd\sigma$, and O1-O2 $pp\sigma$, as well as into direct hopping integrals between Ru (the fact that the fitted values for Ru-Ru hopping do not come from actual overlap of the wave functions is corroborated by the fact that the $dd\delta$ parameters have a far stronger effect on the band structure than the $dd\sigma$ and $dd\pi$ ones). In our notation O1 and O2 describe the in-plane and apical oxygens, respectively. The parameters are listed in Table II. The overall r.m.s. error for this fit is ≈10 mRy for all 18 bands and is less than 2 mRy for the bands crossing the Fermi level (13th to 15th), for which we used a higher weight in order to reproduce the Fermi surface very accurately.

RESULTS

In Fig. 1, we show the TB energy bands of cubic $SrRuO_3$ for both spin up and spin down. We note that the TB bands, especially near the Fermi level (E_F) are almost indistinguishable from the LAPW results of Ref. 1. In the (100) direction we note near E_F a flat band that is occupied for spin-up and above E_F for spin-down. We also see a small electron pocket for spin-up and a gap for spin-down centered

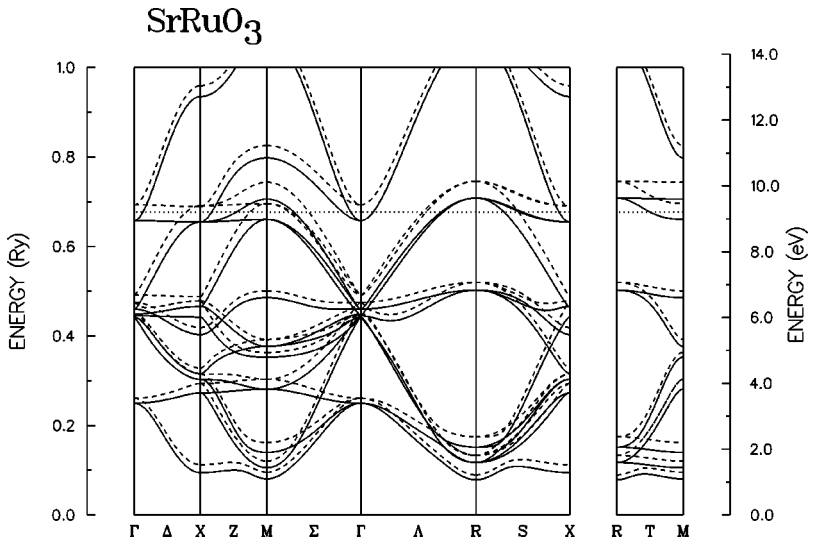

FIG. 1. TB band structure of cubic $SrRuO_3$ for two spin directions.

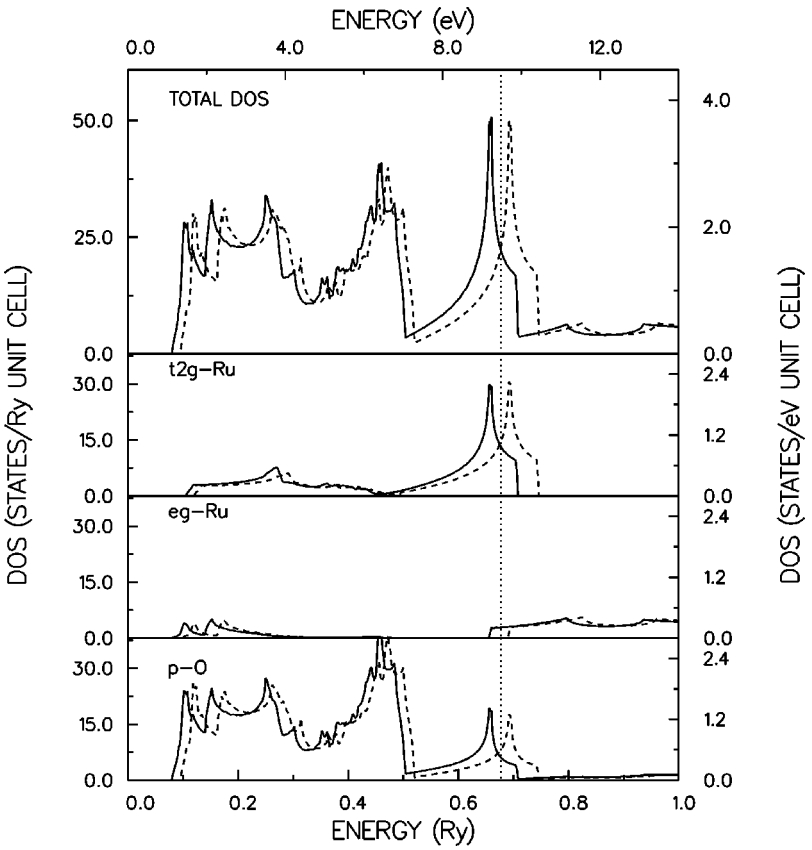

FIG. 2. TB DOS of cubic $SrRuO_3$ for the two spin directions.

at Γ. We observe a hole pocket for spin-down centered at M that vanishes for spin-up. In Fig. 2, we show the TB density of states (DOS) for both spins. In agreement with the LAPW results, we find a pronounced peak just below E_F for spin-up and just above E_F for spin-down, while DOS at E_F is approximately the same for both spins. Both these peaks are a mixture of t_{2g}-Ru and p_π-O states as can be seen from the decomposition of the DOS, in accord with the discussion in Ref. 4. On the other hand, the e_g contribution to DOS at the Fermi level is very small for spin up and nearly zero for the spin down channel.

In Fig. 3, we show a comparison of TB and LAPW energy bands for Sr_2RuO_4. The bands above 2 eV were not fitted. In the low bands far away from E_F there are minor discrepancies. However, the bands near E_F display excellent agreement between TB and LAPW. Note that unlike Ref. 8 the Γ-Z dispersion is rather well reproduced. E.g., the bands at the Z point are almost 1 eV off in Ref. 8, and at the Fermi level the error is several hundreds meV, while our fit produces an accuracy of less than 20 meV for the whole direction. This also results in a virtually perfect match of the Fermi surfaces (Fig. 4). The degree of the nesting of the pseudosquare Fermi surface sheets is reproduced very well, which is crucial for the calculations of susceptibilities and response functions (cf. Ref. 11). Also the (very weak) k_z dispersion, which manifests itself through small violations of the mirror symmetry in Fig. 4, is reproduced.

Apart from computational efficiency, TB models have another advantage with respect to the first-principles methods: electronic velocities, which are usually calculated in the first principles methods by numerical differentiation of electron

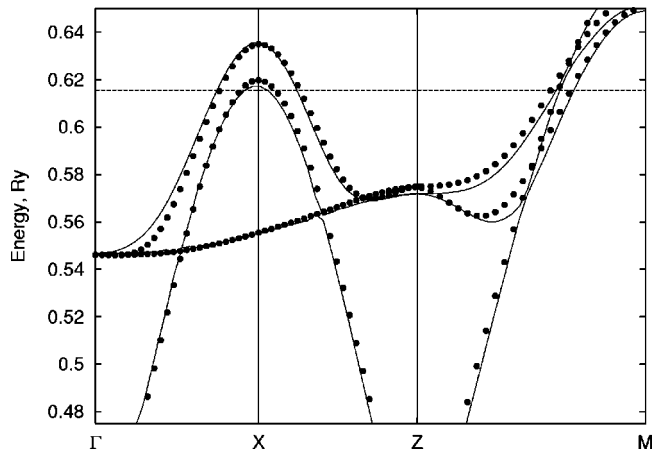

FIG. 3. Band structure of Sr_2RuO_4 in LAPW (circles) and in the TB fit (lines).

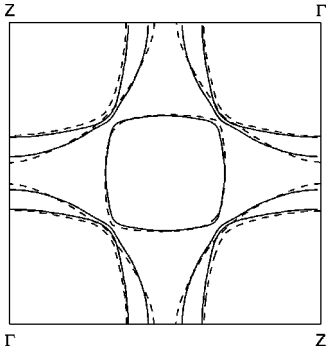

FIG. 4. Fermi surface of Sr_2RuO_4 in LAPW (solid lines) and in the TB fit (dashed lines)

eigenenergies, can be obtained analytically from the TB Hamiltonian without any loss of accuracy

$$\mathbf{v}_{\mathbf{k}i}=\frac{\partial E_{\mathbf{k}i}}{\hbar\,\partial\mathbf{k}}=\left\langle \mathbf{k}i\left|\frac{\partial H}{\partial\mathbf{k}}\right|\mathbf{k}i\right\rangle$$
$$\frac{\partial H}{\partial\mathbf{k}}=\sum_{\mathbf{R}} i\mathbf{R}e^{i\mathbf{k}\mathbf{R}}t_{\mathbf{R}}, \tag{1}$$

where summation is performed over all neighbors for which hopping integrals were included in the Hamiltonian. The first line follows from the Hellman-Feynman theorem, and the second from the TB expression for $H=\Sigma_{\mathbf{R}}e^{i\mathbf{k}\mathbf{R}}t_{\mathbf{R}}$. The advantage of using this formula is particularly clear when there are many band crossings in the energy range of interest, in which case numerical differentiation requires an extremely fine mesh. This is even more true for the physical quantities that depend on an electronic mass (second derivative of the eigenenergy), like Hall coefficient. Since the error of numerical differentiation increases rapidly with the order of the calculated derivative, eliminating the second differentiation by using the Hellman-Feynman velocities is particularly helpful in this case. To illustrate this approach, we computed a quantity that defines the vortex lattice geometry in superconducting Sr_2RuO_4 (Ref. 7) and depends in a non-trivial way on the electronic velocities. Agterberg[7] showed that this geometry is directly related to the symmetry of the order parameter. For an isotropic triplet *p*-wave pairing, one expects a triangular vortex lattice. For a *d* wave pairing a square lattice appears, oriented either along (100) or along (110) directions. It was observed experimentally[12] that in Sr_2RuO_4 Abrikosov vortices form a square lattice; Agterberg[7] performed calculations for a model of a two-dimensional (2D) triplet superconductor, where the angular anisotropy comes entirely from the fermiology. He derived a criterion that controls the geometry of the vortex lattice

$$\nu=\frac{2\langle\delta v^2\rangle^2-\langle v^2\rangle^2}{\langle v^2\rangle^2}=2\frac{\langle v_x^2-v_y^2\rangle^2}{\langle v_x^2+v_y^2\rangle^2}-1. \tag{2}$$

The absolute value of this quantity determines whether the vortex lattice will be triangular or square (for $\nu>0.014$ it is always square), while its sign defines the orientation of the lattice when it is square. If $\nu<0$ it is aligned with the crystal lattice, if $\nu>0$ it is rotated by 45°, as it is observed in the experiment.

Agterberg pointed out that when order parameters are different for the three bands crossing the Fermi level, the actual vortex lattice will be defined by the sign of the weighted ν parameter, which in turn depends on the order parameters Δ in all three bands,

$$\nu_{eff}=(\nu_\alpha\langle v^2\rangle_\alpha^2\Delta_\alpha^2+\nu_\beta\langle v^2\rangle_\beta^2\Delta_\beta^2+\nu_\gamma\langle v^2\rangle_\gamma^2\Delta_\gamma^2)/(\langle v^2\rangle_\alpha^2\Delta_\alpha^2 +\langle v^2\rangle_\beta^2\Delta_\beta^2+\langle v^2\rangle_\gamma^2\Delta_\gamma^2). \tag{3}$$

He estimated, using a three-band TB model of Ref. 5, that $\nu_\alpha\approx\nu_\beta\approx0.6$, while $\nu_\gamma\approx-0.6$ (here the same labeling scheme is used for the Fermi surface sheets that was introduced in Ref. 13). This calculation is to be taken with a grain of salt, though, as the model used for the band structure is rather approximate. However, if indeed $\nu_\alpha\approx\nu_\beta\approx-\nu_\gamma>0$, even a modest interband anisotropy of the order parameter such as that computed in Refs. 5 and 11 can be crucial. Of course, since Eqs. (2) and (3) involve complicated averages over the Fermi surface, the result is very sensitive to the accuracy of the Brillouin zone integration.

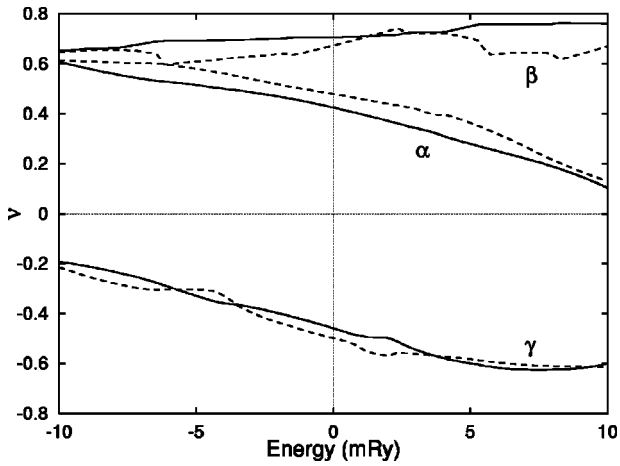

FIG. 5. Anisotropy parameter ν (see text) as the function of the distance to the Fermi level. Solid lines are results of the integration with exact TB velocities, broken lines use velocities from tetrahedron linear interpolation. In both cases $30\times30\times10$ mesh was used.

In Fig. 5, we show the results of our calculation of ν, using the present TB model, Eq. (1), and the tetrahedron integration technique with the 1507 irreducible **k** points in the Brillouin zone. First, we observe that even with such a fine mesh and relatively simple Fermi surface the numerical differentiation of eigenenergies produces noisy curves, compared to the analytical differentiation. Second, we find that there is little dependence of ν on the Fermi energy in the range ±150 meV, although the van Hove singularity is located only 65 meV above the Fermi energy. Third, we see that the calculated values of ν ($\nu_\alpha=0.42$, $\nu_\beta=0.70$, $\nu_\gamma=-0.45$) are not too far from Agterberg's estimates. Fourth, we can use Eq. (2) to estimate the lower limit on the ratio $\Delta_\gamma/\Delta_\alpha$, assuming $\Delta_\alpha=\Delta_\beta$. In order to reproduce the experimental observation that $\nu_{eff}>0$, and using our calculated ratios $\langle v^2\rangle_\alpha:\langle v^2\rangle_\beta:\langle v^2\rangle_\gamma=1.0:0.55:1.0$, we find that $\Delta_\gamma/\Delta_\alpha<1.2$, contrary to the ''orbital-dependent'' superconductivity model.[16]

Another interesting Fermi surface property, which requires highly accurate integration over the Brillouin zone, is the Hall coefficient. It depends on the *second* derivatives of the eigenvalues (see Appendix), which makes numerical differentiation undesirable. We used our TB fit to calculate the Hall coefficient both in diffusive [Eq. (A3)] and ballistic [Eq. (A4)] regimes. Experiments show[14] that the Hall coefficient is negative (electron-like) at $T\to0$, $R=-1.15\times10^{-10}$ m^3/C, but grows rapidly and changes sign at $T\approx35$ K, and stays close to zero at the higher temperatures. It was suggested that this is a manifestation of the different temperature dependence of the relaxation time in different bands.[14] Alternatively, one may think that at $T\sim35$ K a crossover between the two regimes described by Eqs. (A4) and (A3) takes place.

We checked these hypotheses by calculating the conductivities σ_{xy} and σ_{xx} (see Appendix) for all three Fermi surface sheets. In both cases they are calculated up to a common

TABLE III. Conductivities and Hall coefficients in atomic units. The volume of the unit cell $\Omega = 95.4$ Å^3, τ and λ are the relaxation time and the mean free path, respectively. Atomic units for R are such that for a parabolic band $R = 1/n$, where n as given in the first columns is the total number of electrons (α, γ) or holes (β) in the corresponding bands.

Band	n	$\sigma^d_{xx}/\tau\Omega$	$\sigma^b_{xx}/\lambda\Omega$	$\sigma^d_{xy}/\tau\Omega$	$\sigma^b_{xy}/\lambda\Omega$	$R_d\Omega$	$R_b\Omega$	$R_{\exp}\Omega$ ($T=0$)
α	−1.02	2.0	6.0	−4.0	−36	−0.95	−0.98	
β	0.28	1.1	3.2	3.8	32	3.2	3.2	
γ	−1.26	2.0	6.6	−2.8	−30	−0.65	−0.68	
Total	−2.00	5.1	15.2	−3.0	−34	−0.12	−0.15	−0.20

constant factor (constant relaxation time τ or constant mean free path λ). The results were, in atomic units, as given in Table III. First of all, we observe that the difference between the two approximations is very small. Second, we see that the net Hall conductivity originating from the xz/yz sheets of the Fermi surface (α and β, in standard notations) is electronlike. Thus the Mackenzie *et al.* explanation of the sign change at $T \sim 35$ K requires a substantial difference of the temperature dependence of τ_α and τ_β (not only of $\tau_{\alpha,\beta}$ and τ_γ), which is physically hard to support, considering the origin of these bands.

However, as noted in a previous paper,[5] to fit the experimental de Haas-van Alphen extremal area[13] exactly, one has to shift the LDA bands by a few mRy up (α) or down (β, γ). In order to investigate this, we applied shifts of 5, −4, and −1.5 mRy to the bands α, β, and γ, respectively[15] This procedure reduces the energy distance between the van Hove singularity and the Fermi level from ≈65 to ≈20 meV, which makes the difference between the ballistic and the diffusive σ_{xy} more pronounced. The results are shown in Table IV. One immediately observes that now the net Hall conductivity in the bands α and β is *positive*. Thus, if the mean free path in those two bands changes with temperature slower than that for the γ band (to some extent, in spirit of the ''orbital-dependent'' conjecture of Agterberg *et al.*[16]), one may, in principle, expect a sign change of the net Hall coefficient. In fact, one needs to assume that the ratio $\lambda_{\alpha,\beta}/\lambda_\gamma$ increases from ≈1 at $T=0$ to ≈4 at $T \approx 40$ K to explain the observed sign change. This would be unusual, but certainly not impossible.

CONCLUSIONS

To conclude, we presented highly accurate tight-binding fits for cubic $SrRuO_3$ and tetragonal Sr_2RuO_4 perovskites. Using nearest neighbor and a few selected next nearest neighbor hopping parameters we were able to reproduce the first-principles band structure of Sr_2RuO_4 in the physically relevant energy range near the Fermi level with the accuracy of a few mRy. This allows for fast generation of the electronic eigenenergies at a superfine mesh in the Brillouin zone, and fast and virtually exact calculations of the electronic velocities at the same mesh. This powerful technique provides a possibility of investigating physical properties with high sensitivity to the details of the band structure and Fermi surface topology.

We report two applications of the present fit to actual physical problems: First, we calculated the anisotropy parameter ν relevant for the superconducting vortex lattice geometry, and derived from that the lower bound for the interband anisotropy of the order parameter: to ensure compatibility with the experiment, the order parameter in the xy band should not differ more than by 20% from that in the yz/zx bands. Second, we calculated Hall conductivity for the three bands crossing the Fermi level, both in the constant-relaxation-time and in the constant-mean-free-path regimes. Having these numbers we tested the two most natural hypotheses for the temperature-induced sign reversal of the Hall conductivity: crossover between the two above-mentioned regimes and different temperature dependence of the xy- and yz/zx-carrier mobility. We can confidently rule out the former hypothesis. The latter hypothesis cannot be definitely ruled out; for the Fermi surface adjusted to fit the de Haas-van Alphen cross section the desired sign reversal can be obtained in the constant-mean-free-path regimes, if the mean free path for the xy-carriers changes between O K and 40 K at least four times faster than that for the yz/zx-carriers. A possible reason for such a behavior would be substantially stronger electron-paramagnon coupling for the xy electrons.

Finally, we would like to mention that in this paper we presented just two relatively straightforward applications of our TB model. Other, more sophisticated problems that can be attacked with this tool include, for instance, angular-dependent magnetoresistance,[17] Yamaji effect,[18] wave-vector-dependent magnetic susceptibility, and others. We

TABLE IV. The same as Table III, but for the bands shifted to match de Haas–van Alphen cross-section areas.

Band	n	$\sigma^d_{xx}/\tau\Omega$	$\sigma^b_{xx}/\lambda\Omega$	$\sigma^d_{xy}/\tau\Omega$	$\sigma^b_{xy}/\lambda\Omega$	$R_d\Omega$	$R_b\Omega$	$R_{\exp}\Omega$ ($T=0$)
$\alpha 3$	−0.92	2.0	5.7	−4.0	−35	−1.03	−1.05	
$\beta 1$	0.25	1.0	3.0	3.4	37	3.4	4.17	
$\gamma 2$	−1.35	1.9	6.7	−1.8	−29	−0.52	−0.64	
Total	−2.02	4.9	15.4	−3.4	−31	−0.14	−0.13	−.20

emphasize that many of such advanced applications require detailed reproduction of *c* dispersion of the electronic bands, which are highly adequate in the present model, and rather poor in the previous TB models.

Note added in proof. The authors of Ref. 12 have recently discovered that the sample orientation in their experiment was identified incorrectly; we thank Professor E. M. Forgan for sending us this information. In fact, the flux lattice observed in Ref. 12 is not aligned with the crystal axes, but rotated by 45°. Correspondingly, the respective conclusion of our paper should be changed to the opposite: 20% is the upper, not lower boundary on the interband anisotropy of the order parameter in the angularly isotropic *p*-wave model.

ACKNOWLEDGMENTS

We are grateful to D. Agterberg for useful discussions. This work was supported by the Office of Naval Research.

APPENDIX: DERIVATION OF THE HALL FORMULAS

It is convenient to use the 2D expression given by Ong[19]

$$\sigma_{xy}=2\frac{e^2B}{\hbar\Omega}\sum_{\mathbf{k}i}\ \delta(E_{\mathbf{k}i}-E_F)v_y(\mathbf{k}\boldsymbol{\tau})_{\mathbf{k}i}\times\left[v_y(\mathbf{k})\frac{\partial}{\partial k_x}-v_x(\mathbf{k})\frac{\partial}{\partial k_y}\right]v_x(\mathbf{k})\boldsymbol{\tau}_{\mathbf{k}i} \tag{A1}$$

$$\sigma_{xx}=2\frac{e^2}{\hbar\Omega}\sum_{\mathbf{k}i}\ \delta(E_{\mathbf{k}i}-E_F)v_x^2(\mathbf{k})\boldsymbol{\tau}_{\mathbf{k}i}, \tag{A2}$$

which defines the Hall coefficient, $R=-\sigma_{xy}/B\sigma_{xx}^2$. Here Ω is the unit-cell volume, and summation is over all bands and all states in the Brillouin zone. In the constant-relaxation-time approximation this reduces to the following expression:

$$R_d=-\sum_{\mathbf{k}i}\ \delta(E_{\mathbf{k}i}-E_F)(v_x^2\mu_{yy}-v_xv_y\mu_{xy})/2\times\left[\sum_{\mathbf{k}i}\ \delta(E_{\mathbf{k}i}-E_F)v_x^2\right]^2, \tag{A3}$$

where $\mu_{xy}(\mathbf{k})=\partial^2E_{\mathbf{k}}/\partial k_x\partial k_y$, etc. As noticed by Mackenzie *et al.*,[14] at very low temperature a more appropriate approximation is where the mean free path, $v_{\mathbf{k}}\ \boldsymbol{\tau}_{\mathbf{k}}$ is a constant, in which case we have instead

$$R_b=\sum_{\mathbf{k}i}\ \delta(E_{\mathbf{k}i}-E_F)(v_x^2\mu_{yy}-v_xv_y\mu_{xy})v^{-2}/2\times\left[\sum_{\mathbf{k}i}\ \delta(E_{\mathbf{k}i}-E_F)v_x\right]^2. \tag{A4}$$

[1] D. J. Singh, J. Appl. Phys. **79**, 4818 (1996).
[2] D. J. Singh, Phys. Rev. B **52**, 1358 (1995).
[3] T. Oguchi, Phys. Rev. B **51**, 1385 (1995).
[4] I. I. Mazin and D. J. Singh, Phys. Rev. B **56**, 2556 (1997).
[5] I. I. Mazin and D. J. Singh, Phys. Rev. Lett. **79**, 733 (1997).
[6] A. Liebsch and A. I. Liechtenstein, Phys. Rev. Lett. (to be published).
[7] D. F. Agterberg, Phys. Rev. Lett. **80**, 5184 (1999); Phys. Rev. B **58**, 14 484 (1998).
[8] C. Noce and M. Cuoco, Phys. Rev. B **59**, 2659 (1999).
[9] J. P. Julien, D. A. Papaconstantopoulos, D. J. Singh, W. E. Pickett, and F. Cyrot-Lackmann, Physica C **220**, 359 (1994).
[10] D. A. Papaconstantopoulos and W. E. Pickett, Phys. Rev. B **57**, 12 751 (1998).
[11] I. I. Mazin and D. J. Singh, Phys. Rev. Lett. **82**, 4324 (1999).
[12] T. M. Riseman, P. G. Kealy, E. M. Forgan, A. P. Mackenzie, L. M. Galvin, A. W. Tyler, S.-L. Lee, C. Ager, D. M. Paul, C. M. Aegerter, R. Cubitt, Z. Q. Mao, S. Akima, and Y. Maeno, Nature (London) **396**, 242 (1998). The authors have recently discovered that the sample orientation in their experiment was identified incorrectly; we thank Professor E. M. Forgan for sending us this information [E. M. Forgan and D. M. Paul (unpublished)]. The flux lattice observed by them is not aligned with the crystal axes, as originally reported, but rotated by 45°.
[13] A. P. Mackenzie, S. R. Julian, A. J. Diver, G. J. McMullan, M. P. Ray, G. G. Lonzarich, Y. Maeno, S. Nishizaki, and T. Fujita, Phys. Rev. Lett. **76**, 3786 (1996).
[14] A. P. Mackenzie, N. E. Hussey, A. J. Diver, S. R. Julian, Y. Maeno, S. Nishizaki, T. Fujita, Phys. Rev. B **54**, 7425 (1996).
[15] The last number differs from the one in Ref. 5 (3 mRy) because of the difference between the TB fit and the LAPW results.
[16] D. F. Agterberg, T. M. Rice, and M. Sigrist, Phys. Rev. Lett. **78**, 3374 (1997).
[17] E. Ohmichi, H. Adachi, Y. Mori, Y. Maeno, T. Ishiguro, and T. Oguchi, Phys. Rev. B **59**, 7263 (1999).
[18] Y. Yoshida, R. Settai, Y. Onuki, H. Takei, K. Bertsuyaki, and H. Harima, J. Phys. Soc. Jpn. **67**, 1677 (1998).
[19] N. P. Ong, Phys. Rev. B **43**, 193 (1991).